Submitted to the Editor of the Astronomical Journal

A SPECTROSCOPIC STUDY OF LMC X-4

L.D. Petro[1]
Department of Physics and Center for Space Research
Massachusetts Institute of Technology
Cambridge, MA 02139

and

W.A. Hiltner[2]
Astronomy Department
University of Michigan
Ann Arbor, MI 48109

CSR-HEA-82-14

ABSTRACT

The orbital radial velocity semi-amplitude of the LMC X-4 primary is determined to be 37.9±2.4 km s^{-1} from measurements of the hydrogen absorption lines. The semi-amplitude of the He I and He II absorption lines are consistent with this, namely 44.9±5.0 and 37.3±5.3 km s^{-1}. The phase and shape of the radial velocity curves of the three ions are consistent with a circular orbit and an ephemeris based upon X-ray measurements of the neutron star, with the exception that the He II absorption line radial velocity curve has a detectable shape distortion. No effect of the 30-day X-ray cycle on the radial velocity amplitude or spectral type was found, but only half of this cycle is covered by observations. Measurements of the He II λ4686 emission line velocity are consistent with a phase shifted sine wave of semi-amplitude 535 km s^{-1}, a square wave of semi-amplitude 407 km s^{-1}, or high order harmonic fits. The spectral type is found to be O8.5 IV-V during X-ray eclipse. Variations to types as early as O7 occur, but not as a function of orbital phase. Absorption line peculiarities were noted on 6 of 58 spectra.

[1]Present address: Atmospheric and Environmental Research, Inc., 840 Memorial Drive, Cambridge, MA 02139.
[2]Guest investigator Mt. Wilson and Las Campanas Observatories, and Visiting Astronomer Cerro Tololo Interamerican Observatory, operated by the Association of Universities for Research in Astronomy under contract with the National Science Foundation.

I. INTRODUCTION

The LMC X-4 binary system contains a neutron star (Kelley et al. 1982), a massive O-type star (Sanduleak and Philip 1977; Chevalier and Ilovaisky 1977), and probably an accretion disk (Lang et al. 1981, van der Klis et al. 1982). The persistent X-ray luminosity of the neutron star is 7×10^{38} erg s^{-1} in the 13-80 keV band (Lang et al. 1981) and 1×10^{38} erg s^{-1} in the 1-10 keV band (Epstein et al. 1977). The observed X-ray flux is highly modulated at a period of 30.48 days (Lang et al. 1981, Skinner et al. 1980), which is likely caused by a tilted, precessing accretion disk (Lang et al. 1981, van der Klis et al. 1982). The luminosity of the O-star is 5×10^{38} erg s^{-1}, which is slightly less than the luminosity of the neutron star. The visible and ultraviolet brightness of the O-star vary at twice the orbital frequency (Chevalier and Ilovaisky 1977, Bonnet-Bidaud et al. 1980), which is consistent with a tidal distortion origin. The visible light curve is affected by the 30-day modulation, presumably through variable X-ray heating and changing visibility of the accretion disk (Chevalier et al. 1981). The highly luminous X-ray source photoionizes a cavity within the O-star wind which extends to the surface of the O-star and thereby disrupts the formation of the Si IV and N V resonance lines (van der Klis et al. 1982).

It is our purpose in this paper to present measurements of the radial velocity of the O-star and of the He II λ4686 emission line, to make an examination of the velocities and spectra for effects of X-ray heating and the 30-day cycle, and to present a determination of the orbital velocity of the O-star. The data to be discussed were obtained from 58 spectroscopic plates taken with the Cerro Tololo 4-m telescope and the Las Campanas 2.5-m DuPont telescope. These data were combined with velocity measurements from 21 plates presented by Hutchings, Crampton, and Cowley (1978) who made a detailed study of the orbital motion of the O-star.

II. OBSERVATIONS

LMC X-4 was observed by us on three occasions with the Cerro Tololo 4-m telescope and on one occasion with the Las Campanas 2.5-m DuPont telescope. During all four observing runs two-stage, magnetically focussed, second generation Carnegie image tubes (RCA 33063) were used to provide good photographic exposure in the interval λλ3800-4900 Å. A 1 arc-sec entrance slit was employed during all four observing runs.

The Cerro Tololo observations were obtained with the RC spectrograph at a reciprocal linear dispersion of 49 Å mm^{-1}. The width of the entrance slit image in the spectrograph camera focal plane was 39 μm in the direction of dispersion. This corresponds to 1.9 Å or, at the middle of the spectral range, 130 km s^{-1}. Spectra were recorded on unbaked Kodak IIaO plates during the first two observing runs and on baked Kodak IIaO plates during the third run. A typical exposure time was 35 minutes with unbaked plates and 20 minutes with baked plates. The spectra were widened to 1 mm by trailing along the slit. The moonlight eliminator was inoperative during all three runs at Cerro Tololo.

The Las Campanas observations were obtained with a Boller and Chivens spectrograph at a reciprocal linear dispersion of 64 Å mm^{-1}. The width of the entrance aperture image in the spectrograph camera focal plane was 20 μm in the direction of dispersion. However, the measured width of comparison lines is 38 μm, which corresponds to 2.4 Å or, at the middle of the spectral range, 170 km s^{-1}. These spectra were recorded on forming gas baked Kodak IIIaJ plates and were exposed typically for 40 minutes. A tilting quartz block behind the spectrograph entrance aperture was used to widen the spectra to 3/4 mm. The orbital radial velocity semi-amplitude measurement accuracy which we hope to attain is a few kilometers per second, which is approximately 2 per cent of the instrumental FWHM for either spectrograph.

III. RADIAL VELOCITIES

i) Plate Reductions

The goal of the data reduction outlined below is to provide a set of radial velocity measurements and associated standard deviations for hydrogen, helium, and singly ionized helium which are free from instrumental and zero-point effects. Of course, it would be preferable to fit separately the measurements of each line, but the small number (~60) and low precision (σ = 25-100 km s^{-1}) of the present measurements makes such an approach unwarranted.

We have taken some care to identify and remove velocity zero-point errors which are of instrumental origin or the result of an accelerating stellar wind. Variable zero-point errors coupled with the sporadic absence of line measurements (which may be caused by plate flaws or poor exposure) could seriously degrade the quality of the measured orbital velocity. However, no zero-point variability was found, but instead a line velocity error which is an approximately linear function of rest wavelength was found. Our general approach has been to test the smallest natural subsets of the data for zero-point differences and homogeneity of standard deviation. Then, these measurements are combined to form larger data sets which have the mean value subtracted and appropriately formed population standard deviations.

The spectra were measured in one direction with the California Institute of Technology scanning, oscilloscopic Grant measuring engine. Wavelength calibration was accomplished using He-Ar or Fe-Ar spectra which had been exposed above and below each stellar spectrum. The comparison lines have significant curvature caused by the image tubes. We have applied corrections for this curvature which varies between -5 and 5 km s^{-1} as a function of rest wavelength. A polynomial of 3^{rd} or 4^{th} degree was fit to the comparison line laboratory wavelengths as a function of corrected plate position using a

program written by M. Hartoog. The same program used this fit and the O-star effective wavelengths of Conti et al. (1977) to calculate the heliocentric Doppler velocity of each measured stellar line.

The line Doppler velocities were separated by observing run into four groups. From each line velocity the velocity of a trial orbit of 40 km s^{-1} semi-amplitude was subtracted. The period and epoch of this orbit are those determined by Hutchings et al. (1978). The semi-amplitude of the orbit was a compromise between the value of 50 km s^{-1} found by Hutchings et al. (1978) and a preliminary determination of 30 km s^{-1} from the DuPont measurements. The mean and standard deviation of the resulting residuals were computed for each of the four groups. The four values of the mean velocity of a given line are the same to within their respective errors for all of the lines. Surprisingly, an approximately linear trend of mean velocity as a function of rest wavelength is found for each of the four groups. In particular, both the Cerro Tololo and the Las Campanas spectra showed this effect. Because this function is the same for all four runs, the final mean velocity of each line was computed from the average of the four runs. These averages are listed in column 2 of Table 1. The approximate run of velocity is from 240 km s^{-1} near λ3800 Å to 300 km s^{-1} near λ4900 Å. The velocity of the LMC, 274 km s^{-1}, occurs near the middle of the spectrum and suggests an instrumental origin for the effect. The standard deviation of the residuals provide an estimate of the accuracy with which each line was measured. The standard deviation of the Las Campanas measurements was found generally to be twice as great as that of the Cerro Tololo measurements, which were themselves the same for all three runs. These standard deviations are listed in columns 3 and 4 of Table 1.

The next step was to subtract the mean line velocity (V_o in Table 1) from each line Doppler velocity measurement. From the He II λ4686 emission line

velocities 30 km s^{-1} was subtracted, which brings the mean velocity near λ4686 A into agreement with the LMC velocity (274 km s^{-1}). The weighted average plate velocity and its standard deviation for the hydrogen, helium I and helium II ions were calculated using:

$$v_{ion} = \sum_i (v_i - V_o)\, w_i \,/ \sum_i w_i$$

$$(\sigma^2_{ion})^{-1} = \sum_i \sigma_i^{-2}$$

The weight of a line velocity is $w_i = 1/\sigma_i^2$. The sums extend over the available measurements on each plate of the lines of the particular ion. Only those lines listed in Table 1 were used. It should be noted that the standard deviation assigned to each plate velocity depends upon the population standard deviations of the lines forming that mean velocity and not upon the r.m.s. of the small number of line measurements on that plate, which is a more stable procedure. These results are listed in columns 4-10 of Table 2, along with the heliocentric Julian Date (column 1), the spectral class (column 2), and the He II λ4686 emission strength (column 3). The latter two quantities will be discussed in Section IV.

To combine our measurements with those of Hutchings et al. (1978), it is necessary to subtract from their measurements the appropriate mean velocities and to determine the standard deviation of their hydrogen, helium I and helium II velocities. Weighted least squares fits of $v(\theta) = A_o + S_1 \sin\theta$ were made to the data using the relative weights reported by Hutchings et al. (1978). The standard deviation of a plate of unit weight was adjusted until the reduced chi-squared (χ^2_ν) was 1.0. For the hydrogen line fit we noted that half of the variance was contributed by two measurements which deviated by more than 3σ from the best fit. These two measurements were removed and the

final standard deviation and mean velocity were determned. The resulting standard deviations were found to be comparable to those of the Cerro Tololo spectra obtained by us. The standard deviation of a plate of unit weight was found to be, for hydrogen, helium I and helium II 20 km s^{-1}, 44 km s^{-1}, and 26 km s^{-1}. For hydrogen and neutral helium the range of weights is 1-3 and for helium II all plates have equal weight. For the fits to be reported below the best-fit mean velocity for each of the three ions has been subtracted from each plate velocity.

ii) Absorption Line Radial Velocity Fits

We have used the data reported in Table 2 combined with that of Hutchings et al. (1978) to determine best-fit values for the radial velocity semi-amplitude of circular orbits, to test for variability of the radial velocity amplitude, to test for orbital ellipticity, to test for phase shifts from the ephemeris of Hutchings et al. (1978), and to test for distortion of the radial velocity curves. All fits were made using an orbital period (P) equal to 1.40830 d and epoch (T_o) of mid-X-ray eclipse equal to JD 2,443,476.400 (Hutchings et al. 1978). To discuss our results we shall define, for an observation made at time t, $\theta = 2\pi\,(t-T_o)/P$ and the phase, $\phi = \theta/2\pi$. These phases will be referred to as "X-ray phases".

Before carrying out the tests listed above, we fit the hydrogen velocity measurements to $v(\theta) = A_o + S_1 \sin\theta + C_1 \cos\theta$ for a range of trial orbital periods. The period with minimum χ^2 is consistent with the period given by Hutchings et al. (1978). We note that the ephemeris of Hutchings et al. (1978) and Kelley et al. (1982), which is based upon an analysis of X-ray eclipse observations of the neutron star, differ by less than 0.01 in phase at the times of the observations considered here.

The hypothesis testing formalism that we have employed is the F-test (Bevington 1969). The F statistic is defined as the ratio of two reduced chi-squared statistics which have μ and ν degrees of freedom: $F_{\mu\nu} = \chi^2_\mu/\chi^2_\nu$. If this ratio differs significantly from 1, then it is reasonable to chose one of the fits over the other. The standard deviations of the observations will not be as important as the suitability of the fitting functions in forming this ratio if the same data set is employed for both fits. It will be convenient when comparing fits with different numbers of free parameters to take advantage of the fact that the difference of χ^2 statistics, with μ and ν degrees of freedom, is itself a chi-square statistic with $\mu-\nu$ degrees of freedom.

Table 3 contains the result of testing for variability of the orbital radial velocity amplitude. To perform this test the data were divided into five time ranges as shown in Table 3a. For the data sets at hand these correspond to nearly non-overlapping ranges of 30-day phase, as shown in the third column of Table 3a. Therefore the test we have performed can be regarded as a test of variability as a function of 30-day phase or as a function of time. Weighted least squares fits of the function $v(\theta) = A_o + S_1 \sin\theta$, with A_o and S_1 as free parameters, were made to the five individual data sets and to the union of these five data sets. These six fits may be used to calculate χ^2 for two hypotheses: 1) the amplitude and velocity zero-point are not variable and 2) the amplitude and velocity zero-point are variable. The second through fourth columns of Table 3b give the resulting values of χ^2_ν and the numbers of degrees of freedom for fits based upon these two hypotheses. To test whether the hypothesis of variability leads to significant reduction of χ^2, we computed the value of the F statistic defined by: $F_{12} = (\Delta\chi^2/\Delta\nu)/(\chi^2_1/\nu_1)$ where $\Delta\chi^2 = \chi^2_1 - \chi^2_2$ and $\Delta\nu = \nu_1 - \nu_2$. For the hypothesis

of variability χ^2 is simply calculated as the sum of the values of χ^2 for the five individual fits. We have adopted the criterion of not accepting the second hypothesis unless there is less than a 1% probability ("2.6 σ") of the observed value of F occurring by chance alone. By this criterion only helium II shows amplitude variability. Examination of the helium II fits to the 5 data sets shows that this result arises from a very large (162 ± 26 km s^{-1}) semi-amplitude from the small (7 observation) third data set. We therefore do not regard the variability as a significant result although it does satisfy our statistical criterion.

Adopting the hypothesis of non-variability for each of the three ions, we have fit all the available observations to determine the best circular orbit parameters. These results are shown in Figure 1 and are listed in Table 4. We note that the helium I and helium II semi-amplitudes are consistent with that of hydrogen.

We have tested for harmonic components through the third harmonic. These results are shown in Table 5. If one additional term is included, no significant reduction in χ^2 is found for hydrogen and helium I. For helium II, inclusion of a cos 3θ term or a cos 4θ term significantly reduces χ^2. We note that the inclusion of a cos θ term in the fitting function, which corresponds to a shift of epoch, does not lead to significant reduction of χ^2 for any of the ions. Simultaneously fitting the fundamental and first harmonic functions, such as an elliptic orbit would require, does not lead to significant reduction of χ^2. If we take the 2σ ranges of these coefficients, then the limit on the orbital eccentricity is $e \lesssim 0.23$.

iii) <u>He II λ4686 Emission Line Fits</u>

We have fit the 38 radial velocity measurements of the He II λ4686 emission line following procedures similar to those described above for the

absorption line velocities. Equal weights were adopted for all the velocity measurements. The results are displayed in Table 6 and Figure 2. First, $v(\theta) = A_o + S_1 \sin\theta$ was fit to the data. Visual inspection of this fit suggested that a phase shift exists between the data and the fit. Fitting $v(\theta) = A_o + S_1 \sin\theta + C_1 \cos\theta$ significantly reduces χ^2 and is shown in Figure 2 as a solid line. This fit implies that the He II λ4686 emission site lags the neutron star by 0.069 ± 0.012 in phase. We have arbitrarily adopted this as a reference fit and adjusted the standard deviation of the measurements until $\chi^2_\nu = 1.0$. We also rejected two velocities, as shown in Figure 2, because they deviated by ~600 km s^{-1} from the fit. The standard deviation is determined to be 108 km s^{-1}. As Table 6 shows, the additional harmonic term sin 3θ provides significant reduction of χ^2. Furthermore, inspection of Figure 2 suggested that a square wave velocity variation might provide a good representation of the data. This is confirmed by a fit of the function

$$v(\phi) = v_+ \quad ; \; 0.6 \leq \phi \leq 1.0$$
$$= v_- \quad ; \; 0.0 < \phi < 0.6 \; .$$

The best-fit values are 687 km s^{-1} for v_+ and -126 km s^{-1} for v_-, which yields a semi-amplitude of 407 km s^{-1} and a mean velocity of 281 km s^{-1}. To compare this fit with the harmonic fits we make the conservative assumption that the phases of the square wave transitions are free parameters and thereby adopt 34 degrees of freedom for the fit. Reduced chi-squared is then 0.76 for the square wave fit which is to be compared with 0.71 for the best harmonic fit (which also has 34 degrees of freedom) and 1.04 for the best (phase shifted) circular orbit fit. Thus, the square wave is as good a representation as the best harmonic function fit and significantly better than the (phase shifted) circular orbit fit.

IV. THE SPECTRUM

We have examined the 58 spectra obtained by us to determine, wherever possible, the spectral class and the strength of He II λ4686 emission and to search for pecularities. These results are given in columns 2, 3 and 11 of Table 2 and are shown in Figure 3.

Chevalier and Ilovaisky (1977) and Hutchings et al. (1978) have reported that the spectrum of LMC X-4 varies in a systematic fashion with orbital phase. However, Chevalier and Ilovaisky have found the functional dependence to be sin θ with earliest spectral type at phase 0.5, whereas Hutchings et al. (1978) find a sin 2θ dependence with earliest spectral type at quadratures. Figure 3a demonstrates that a persistent sin θ or sin 2θ variation of spectral type with orbital phase does not exist. If any systematic characterization of Figure 3a can be given, it is that there is less spectral variability in the phase interval 0.6-1.0 than in the interval 0.2-0.5. The range of variability is O7-O9. Although there does not appear to be a persistent pattern of spectral type variability, we do note that the data obtained at Las Campanas in the interval JD 2443467-73 could be represented by a sin θ variation. This is of interest because these data are contiguous with those of Hutchings et al. (1978) who found a sin 2θ variation. We have visually examined individual plots of spectral type as a function of orbital phase [Sp (φ)] for the four observing runs made by us. There is insufficient data in these plots to draw firm conclusions, but no significant correlation of the shape of Sp (φ) with 30-day phase is apparent.

The strength of the He II λ4686 emission was estimated relative to the absorption strength of He II λ4686 and this is tabulated in column 3 of Table 2. If the absorption line was not visible no estimate is entered in Table 2. As Figure 3b shows, the He II λ4686 emission strength follows a sin 2θ

variation as found by Chevalier and Ilovaisky (1977) and Hutchings et al. (1978). The maximum strength is 1.5 times that of the absorption line and occurs at quadratures. The minimum line strength is zero, occuring at both conjunctions. However, there are occasions when emission is clearly visible at phase 0.5. The He II λ4686 emission is more often visible in the interval 0.5 - 1.0 than in the interval 0.0 - 0.5. We searched for a 30-day dependence of the emission strengths in the same manner as we searched for a spectral type variation. Again, there were insufficient data to draw any conclusions.

The spectral type of the O-star was determined following the work of Walborn (1971, 1972, 1973, 1977) on classification of O-stars and with respect to spectra published by Walborn (1971, 1973, 1977) and by Morgan, Abt, and Tapscott (1978). To minimize the influence of the X-ray heated portion of the O-star atmosphere we examined four spectra which were taken during X-ray source eclipse. We find the spectral type to be O8.5 IV-V. The spectral class O8.5 is determined by the strength of He II λ4541 relative to He I λ4471 and by the near absence of He II λ4200 with respect to He I/He II λ4026. The possible range of luminosity class is determined by the presence of Si IV λ4089 and N II λ4514/15 which have a positive luminosity effect, the weakness of He I λ4387 and He II λ4686 which have a negative luminosity effect, the near absence of C III λλ4647-51 which has a positive luminosity effect, and the breadth of the hydrogen lines.

We have noted peculiarities in 6 spectra. In two spectra He II λ4541 appears narrow (approximately half the width of He I λ4471) and deep, in four spectra He II λ4541 appears broad (approximately twice the width of He I λ4471), and in one spectrum Si IV λ4089 and He I λ4144 are strongly present.

V. DISCUSSION

We have presented here a determination of the orbital radial velocity of the O-star companion of LMC X-4 and the results of testing for non-orbital effects. Heating effects, such as those discussed by Milgrom (1977), are notably absent in the orbital phase-radial velocity plots. Visual inspection of Figure 1 and harmonic fits (Table 5) demonstrate that the hydrogen and helium I radial velocity curves do not show an enhancement of the radial velocities in the phase interval 0.75-0.25 as predicted by Milgrom (1977). Because the hydrogen fits do not show radial velocity amplitude variability which is correlated with 30-day phase and because they are of better statistical quality than the He I fits we adopt the hydrogen semi-amplitude as providing the best estimate of the orbital radial velocity. Although we have not been able to detect variability of amplitude or to detect harmonic distortion of the radial velocity curve, we naturally cannot exclude the possibility of a non-variable distortion which is in phase with and at the frequency of the orbital motion. The determination of the dynamical parameters of the binary system using this orbital velocity measurement has been made elsewhere (Kelley et al. 1982).

In Section III.iii we have presented harmonic and square wave fits to the He II λ4686 emission line radial velocity measurements which we believe must be viewed with caution. The edges of a rotationally broadened stellar He II λ4686 absorption line extend 380 km s^{-1} from line center. We have indicated these edges (assuming V_o = 274 km s^{-1}) in Figure 2. It is apparent that the measurements of the He II λ4686 emission velocity cluster just outside these limits. This suggests that blending of the absorption and emission components has a strong effect on the measurement of the emission line velocity. We believe that only qualitative information may be derived from the He II

emission line velocities presented in Figure 2. The data show that the emission is more often visible around phase 0.8 than around phase 0.3, that the phases of visibility lag the phases of the neutron star radial velocity extrema, and that the radial velocity amplitude (800-1000 km s^{-1}) of He II λ4686 is comparable to that of the neutron star (~930 km s^{-1}, Kelley et al. 1982).

The variable spectral class of the LMC X-4 primary is in approximate agreement with the temperatures of its heated and unheated hemispheres as a simple calculation based upon the X-ray luminosity and O-star solid angle shows. However, variability of spectral class and luminosity class also have been observed in the Cyg X-1 primary (Smith et al. 1973) and of spectral class in the Cen X-3 and SMC X-1 primaries (Hutchings et al. 1977, Hutchings et al. 1979). Because significant heating of the Cyg X-1 and Cen X-3 primaries does not occur, the existence of spectral variability in these systems suggests that causes other than X-ray heating are important.

We have observed spectrum peculiarities near both conjunctions and both quadratures. The strengthening of Si IV λ4089 and He I λ4144 occurred on a single plate at phase 0.80 with adjacent exposures not revealing a similar affect. It is interesting to note that the time scale of this event (approximately one-half hour) is approximately the same as the time scale of X-ray flares such as those first observed by Epstein et al. (1977). Broadening of He II λ4541 occurred near phase 0.22 and phase 0.80. We do not find persistent broadening of He II λ4541 near phase 0.80 as proposed by Hutchings et al. (1978) as evidence for the existence of a wake.

The observed pattern of He II λ4686 visibility and strength variation is similar to that reported for SMC X-1 (Osmer and Hiltner 1974) and for Cyg X-1 (Smith et al. 1973, Walker et al. 1978).

We would like to thank NASA for its support of this work through grants NAS5-24441 and NGR 23-005-464. One of us (L.P.) would like to thank the Carnegie Institution of Washington for the tenure of a fellowship during which time the Las Campanas observations were obtained and the major portion of the analysis completed.

REFERENCES

Bevington, P.R. (1969). Data Reduction and Error Analysis for the Physical Sciences, (New York: McGraw-Hill).

Bonnet-Bidaud, J.M., Glencross, W.M., Willis, A.J., Hammerschlag-Hensberge, G., van der Klis, M., Ilovaisky, S.A., and Mouchet, M. 1980, in Proceedings of Second European IUE Conference (ESA SP-157), p. 173.

Chevalier, C. and Ilovaisky, S. (1977). Astr. Ap., 59, L9.

Chevalier, C., Ilovaisky, S.A., Motch, C., Pakull, M., Lub, J., and van Paradijs, J. (1981). Sp. Sci. Rev., 30, 405.

Conti, P.S., Leep, E.M., and Lorre, J.J. (1977). Ap. J., 214, 759.

Epstein, A., Devaille, J., Helmken, H., Murray, S., Schnopper, H.W., Doxsey, R., and Primini, F. (1977). Ap. J., 216, 103.

Hutchings, J.B., Cowley, A.P., Crampton, D., van Paradijs, J., and White, N.E. (1979). Ap. J., 229, 1079.

Hutchings, J.B., Crampton, D., and Cowley, A. (1978). Ap. J., 225, 548.

Hutchings, J.B., Crampton, D., Cowley, A.P., and Osmer, P.S. (1977). Ap. J., 217, 186.

Kelley, R.L., Jernigan, J.G., Levine, A., Petro, L.D., and Rappaport, S. (1982). submitted to Ap. J.

Lang, F.L. et al. (1981). Ap. J. (Letters), 246, L21.

Milgrom, M. (1977). Astr. Ap., 54, 725.

Morgan, W.W., Abt, H.A., and Tapscott, J.W. (1978). Revised MK Spectral Atles for Stars Earlier than the Sun, (Yerkes Observatory, Univ. of Chicago and Kitt Peak National Observatory).

Osmer, P.S. and Hiltner, W.A. (1974). Ap. J. (Letters), 188, L5.

Sanduleak, N., and Philip, A.G.D. (1977). I.A.U. Circular No. 3023.

Skinner, G.K. et al. (1980). Ap. J., 240, 619.

Smith, H.E., Margon, B., and Conti, P.S. (1973). Ap. J. (Letters), 179, L125.

van der Klis, M. et al. (1982). Astr. Ap., 106, 339.

Walborn, N.R. (1971). Ap. J. Supp., 23, 257.

Walborn, N.R. (1972). A.J., 77, 312.

Walborn, N.R. (1973). A.J., 78, 1067.

Walborn, N.R. (1977). Ap. J., 215, 53.

Walker, G.A.H., Yang, S., and Glaspey, J.W. (1978). Ap. J., 226, 976.

FIGURE CAPTIONS

Figure 1: Measurements and best circular orbit fits of the radial velocities of the LMC X-4 primary. The mean velocity has been subtracted from all measurements. Symbols used are: Cerro Tololo 4-m observations reported here and by Hutchings et al. (1978), Las Campanas 2.5-m observations, * observations not included in the fit. Observations marked by arrows lie beyond the figure boundary.

Figure 2: Measurements and fits of the radial velocities of the He II λ4686 emission in the LMC X-4 system. The best-fit sine function (solid curve) lags the neutron star by 25°. The best-fit unshifted sine function is drawn as a dotted curve. The limits of a rotationally broadened stellar λ4686 absorption line are indicated by the two horizontal dashed lines. Symbols used are: Measurements reported here from the CTIO 4-m telescope and the Las Campanas 2.5-m telescope and those of Hutchings et al. (1978), * measurements excluded from the fit.

Figure 3: a) Spectral class of the LMC X-4 primary from Table 2. Symbols used are: CTIO 4-m telescope, Las Campanas 2.5-m telescope. b) He II λ4686 emmission strength relative to He II λ4686 absorption line strength.
The dashed vertical lines are drawn at the phases of X-ray eclipse ingress and egress.

Table 1

Mean and Standard Deviation of Absorption Line Velocity Measurements

Line	V_o (km s^{-1})	Standard Deviation Cerro Tololo (km s^{-1})	Las Campanas (km s^{-1})
H9	236	30	60
Hβ	262	26	52
Hε	229	36	74
He I λ4026	285	46	49
Hδ	259	23	47
He II λ4199	281	52	114
Hγ	284	23	47
He I λ4387	355	79	84
He I λ4471	303	46	49
He II λ4541	311	52	114
He II λ4686	298	30	66
He I λ4713	324	79	84
Hβ	296	26	52

Table 2

Journal of Observations

HJD -2443000	Sp	λ4686e / λ4686a	Hydrogen v	Hydrogen σ	Helium I v	Helium I σ	Helium II v	Helium II σ	λ4686e v	Remark
a) Cerro Tololo Observations										
197.539	08	0	-15	14	-25	29	5	26	-	
197.570	09	-	-19	14	-2	28	4	26	-	λ4686 filled in
197.597	09	-	-8	14	24	40	-22	56	-	" "
197.624	08.5	-	29	14	10	40	-36	23	-	He II λ4541 sharp, λ4686 filled in
198.535	08	1	-46	13	-86	29	-59	23	668	
198.563	08.5	3/2	-19	14	-104	29	-35	23	639	
198.591	08.5	3/2	-51	14	-42	28	-43	23	745	
198.618	08.5	1	-26	13	-64	28	-51	26	621	
199.523	-	0	17	11	-44	29	-11	23	-	
199.562	-	0	17	13	-25	29	-6	23	-	
199.589	09	1/4	4	11	-3	29	5	23	640	
199.619	09	1/4	5	11	-45	28	27	23	591	
215.516	08	1/2	-42	11	8	28	-8	23	649	
215.541	08.5	1/4	-33	11	-44	28	-41	23	668	
215.564	08.5	1/2	-48	11	-10	28	-13	23	679	
215.585	09	1	-7	11	-22	29	-17	23	663	Si IV λ4089 and He I λ4144 strong, He II λ4541 sharp
215.730	-	1	-20	14	45	40	5	23	578	
216.513	08	1	-1	11	-22	29	54	23	-141	
216.532	07.5	1/2	9	11	12	29	35	23	-163	He II λ4541 sharp
216.557	07.5	1/2	7	11	-4	29	34	23	-202	
216.580	07.5	1/2	22	11	4	29	37	23	-139	
216.605	08	0	5	11	12	29	12	23	-	
217.519	08.5	1	37	11	3	29	58	23	-171	
217.538	08	3/2	34	11	31	29	52	23	-164	
217.562	07.5	3/2	46	11	48	29	62	23	-112	He II λ4541 broad
217.584	07.5	3/2	33	11	66	29	66	23	-196	"
217.605	07.5	3/2	43	11	78	28	44	23	-173	"
465.757	08.5	0	29	11	-9	28	30	26	-	
465.793	08.5	1/2	7	11	59	29	91	23	-87	
465.834	0.85	0	19	12	14	29	76	23	-	
467.754	-	-	-	-	-	-	-	-	679	λ4686 filled in
467.788	08.5	-	-15	11	-138	44	-153	29	-	" " "
467.805	09	1	-30	11	4	32	-38	26	611	
467.827	08.5	1/2	-16	11	-8	32	-31	29	-	
467.845	08.5	1/2	-33	11	-20	29	16	51	688	

b) Las Campanas Observations

467.808	09:	-	8	22	-68	49	106	81	-
468.720	-	-	7	24	-77	32	-21	57	-
469.545	09:	1	15	28	-17	32	-	-	-
469.616	09:	1	54	22	34	32	-38	114	-130
469.834	07	1/2	24	22	42	42	50	57	-151
470.577	-	-	11	27	-22	32	-	-	-
470.607	-	-	-54	24	68	49	-	-	-
470.691	-	-	28	24	12	32	-51	57	-
470.710	-	-	15	24	0	32	-97	52	-
470.794	09	-	-22	24	35	34	7	114	-
471.591	08	0	38	22	-21	30	-94	57	-
471.620	08	0	4	24	-84	34	-93	52	-
471.696	08.5	1	-71	23	-38	32	-93	81	714
471.724	08.5	-	-38	24	-37	32	-97	81	-
471.753	08.5	1	-48	22	-51	32	-2	57	572
471.783	08.5	1	-27	25	1	32	18	52	-
472.611	08.5	-	33	22	32	32	-22	66	-
472.655	08.5	1/2	-2	22	24	32	-17	57	-152
472.771	08	-	-8	22	-25	32	-72	57	-
472.801	08	1/2	-11	22	-14	38	82	52	-328
473.615	08.5	-	-32	24	29	32	2	114	-
557.602	08	3/4	-	-	-	-	-	-	-
559.570	08	1	-	-	-	-	-	-	-

Table 3

Test of Orbital Radial Velocity Amplitude Variability

a) Data Sets

Group	Time Range (JD-2443000)	30-day Phase*	Number of Observations H	He I	Ne II
1	197-199	0.41-0.48	12	12	12
2	215-217	0.00-0.19	15	15	15
3	465-467	0.21-0.28	7	7	7
4	467-473	0.28-0.47	21	21	18
5	472-479	0.41-0.64	14	17	12

*P = 30.48 d, T_o = JD 2443368 (Lang et al. 1981).

b) Fit of $v(\theta) = A_o + S_1 \sin\theta$

Ion	constant amplitude ν	constant amplitude χ^2_ν	variable amplitude ν	variable amplitude χ^2_ν	$\Delta\nu$	$*F_{\Delta\nu,\nu}$
Hydrogen	67	1.178	59	1.183	8	0.97
Helium I	70	1.282	62	1.107	8	2.06
Helium II	62	1.786	54	1.038	8	3.83

* The observed value of $F_{\Delta\nu,\nu}$ must exceed 2.8 for there to be less than 1% probability of chance occurrence.

Table 4

Best Fit Circular Orbit Parameters

Ion	ν	χ^2_ν	A_o (km s^{-1})	S_1 (km s^{-1})
Hydrogen	71	1.159	1.2 ± 1.6	37.9 ± 2.4
Helium I	74	1.252	-2.8 ± 3.5	44.9 ± 5.0
Helium II	66	1.698	6.2 ± 3.7	37.3 ±5.3

Table 5

Tests of Additional Terms*
$v(\theta) = A_o + S_1 \sin\theta + f(\theta)$

f(θ)	Hydrogen (ν = 71) Δν	Hydrogen (ν = 71) $F_{\Delta\nu,\nu}$	Helium I (ν = 74) Δν	Helium I (ν = 74) $F_{\Delta\nu,\nu}$	Helium II (ν = 66) Δν	Helium II (ν = 66) $F_{\Delta\nu,\nu}$
cos θ	1	2.87	1	0.92	1	4.64
sin 2θ	1	0.83	1	1.43	1	0.001
cos 2θ	1	0.43	1	0.18	1	0.51
sin 3θ	1	0.55	1	0.20	1	0.52
cos 3θ	1	2.87	1	1.90	1	11.40
sin 4θ	1	2.39	1	1.39	1	0.02
cos 4θ	1	0.03	1	5.35	1	10.97
elliptic*	3	1.58	3	0.94	1	1.57

* The observed value of $F_{\Delta\nu,\nu}$ must exceed 7.0 for Δν=1 and 4.1 for Δν=3 for there to be less than 1% probability of chance occurrence.

* For the elliptic orbit fit, $f(\theta) = C_1 \cos\theta + S_2 \sin 2\theta + C_2 \cos 2\theta$.

Table 6

He II λ4686e Harmonic Fits

Function*	ν_1	χ^2_ν	F_1^*	A_o	S_1	C_1	S_3
f_1	36	2.72	-	210±18	-509±22	-	-
f_2	35	1.04	22.50	223±18	-486±23	225±28	-
f_3	34	0.71	11.15	256±20	-457±24	276±29	92±27

*$f_1(\theta) = A_o + S_1 \sin\theta$; $f_2(\theta) = f_1(\theta) + C_1 \cos\theta$; $f_3(\theta) = f_2(\theta) + S_3 \sin 3\theta$

*$F_2 = (\chi_1^2 - \chi_2^2)/\chi_1^2$; $F_3 = (\chi_2^2 - \chi_3^2)/\chi_2^2$.

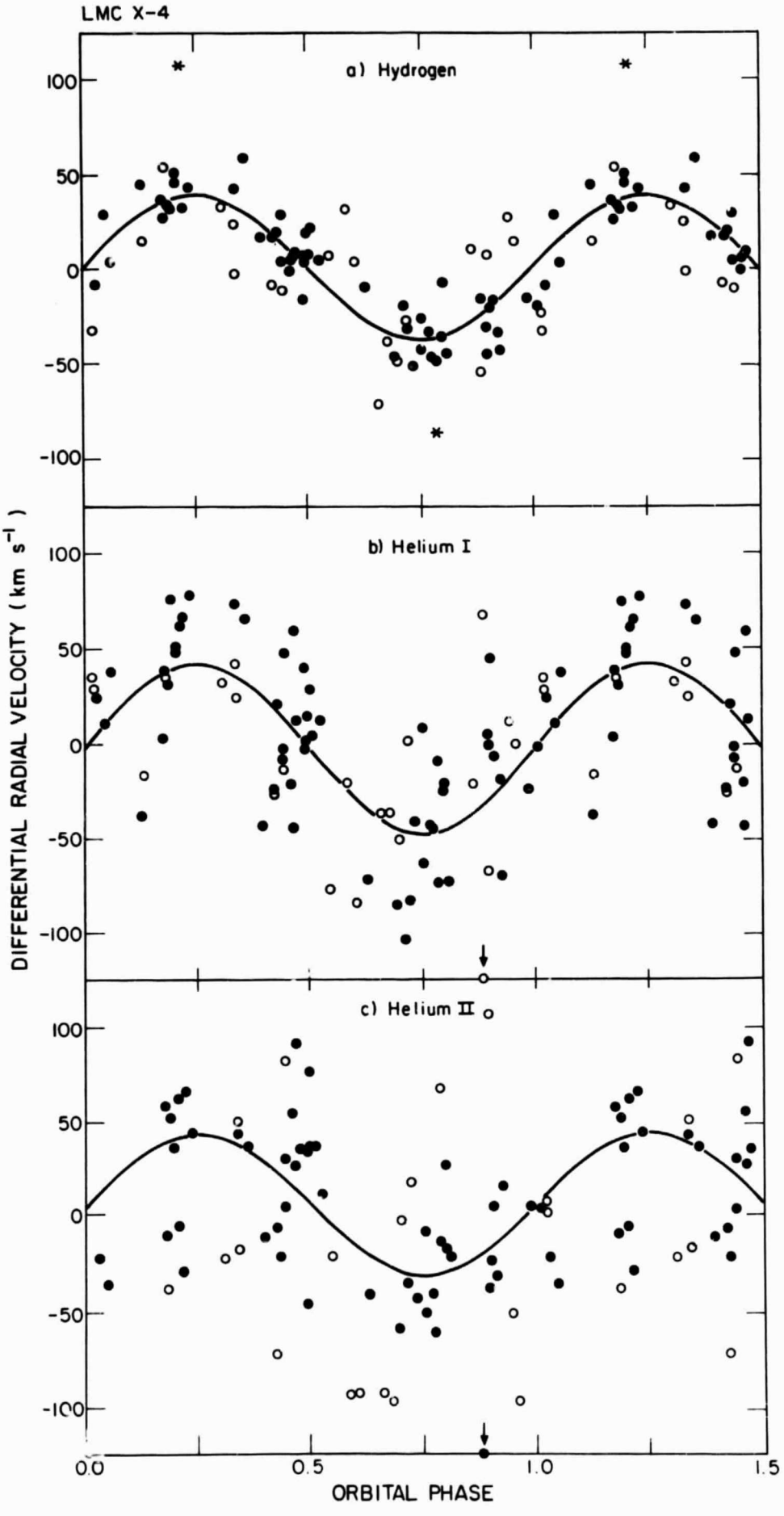
LMC X-4
a) Hydrogen
b) Helium I
c) Helium II
DIFFERENTIAL RADIAL VELOCITY (km s^{-1})
ORBITAL PHASE
100
50
0
-50
-100
0.0
0.5
1.0
1.5

Figure 1

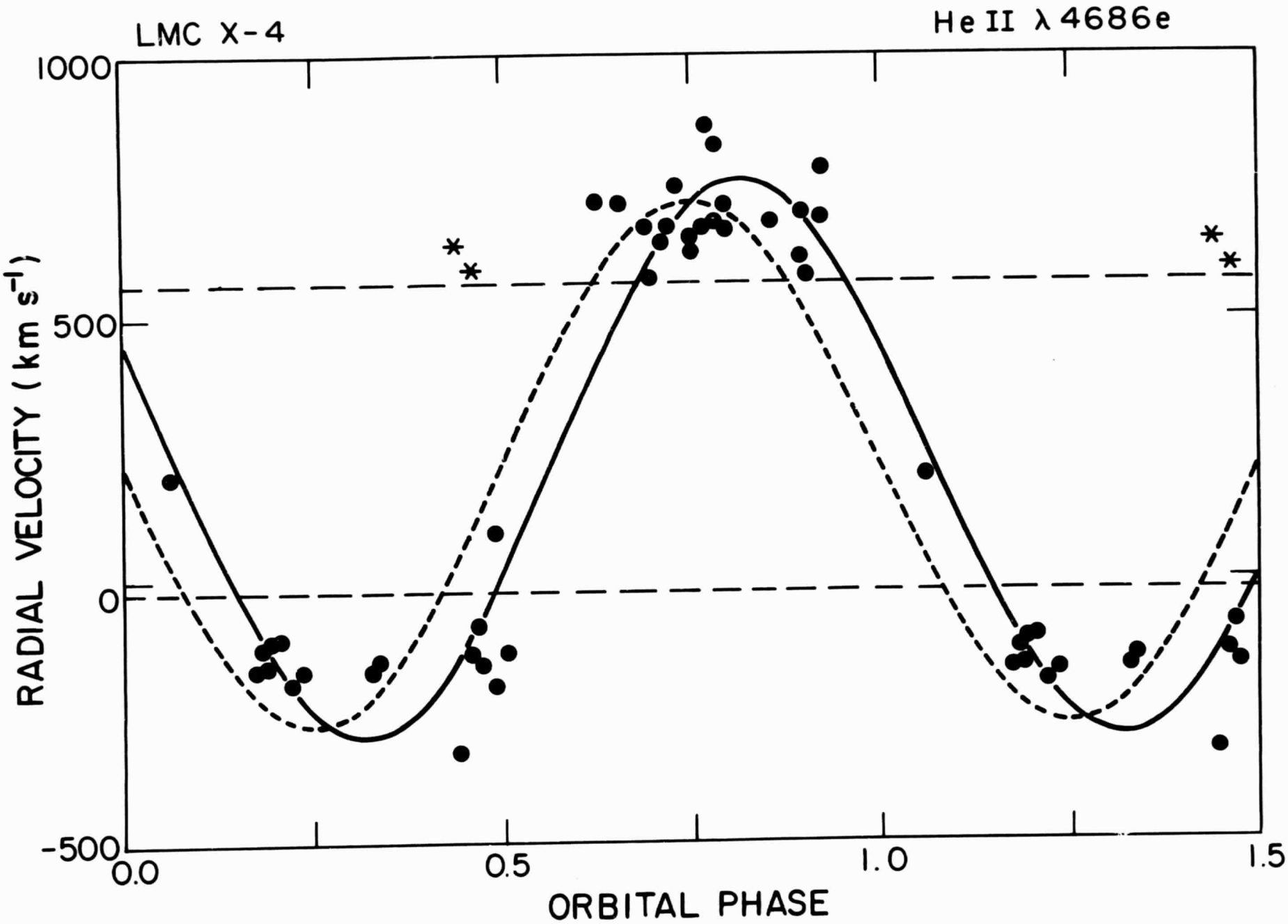
LMC X-4
He II λ4686e
1000
500
0
-500
RADIAL VELOCITY (km s⁻¹)
0.0
0.5
1.0
1.5
ORBITAL PHASE

Figure 2

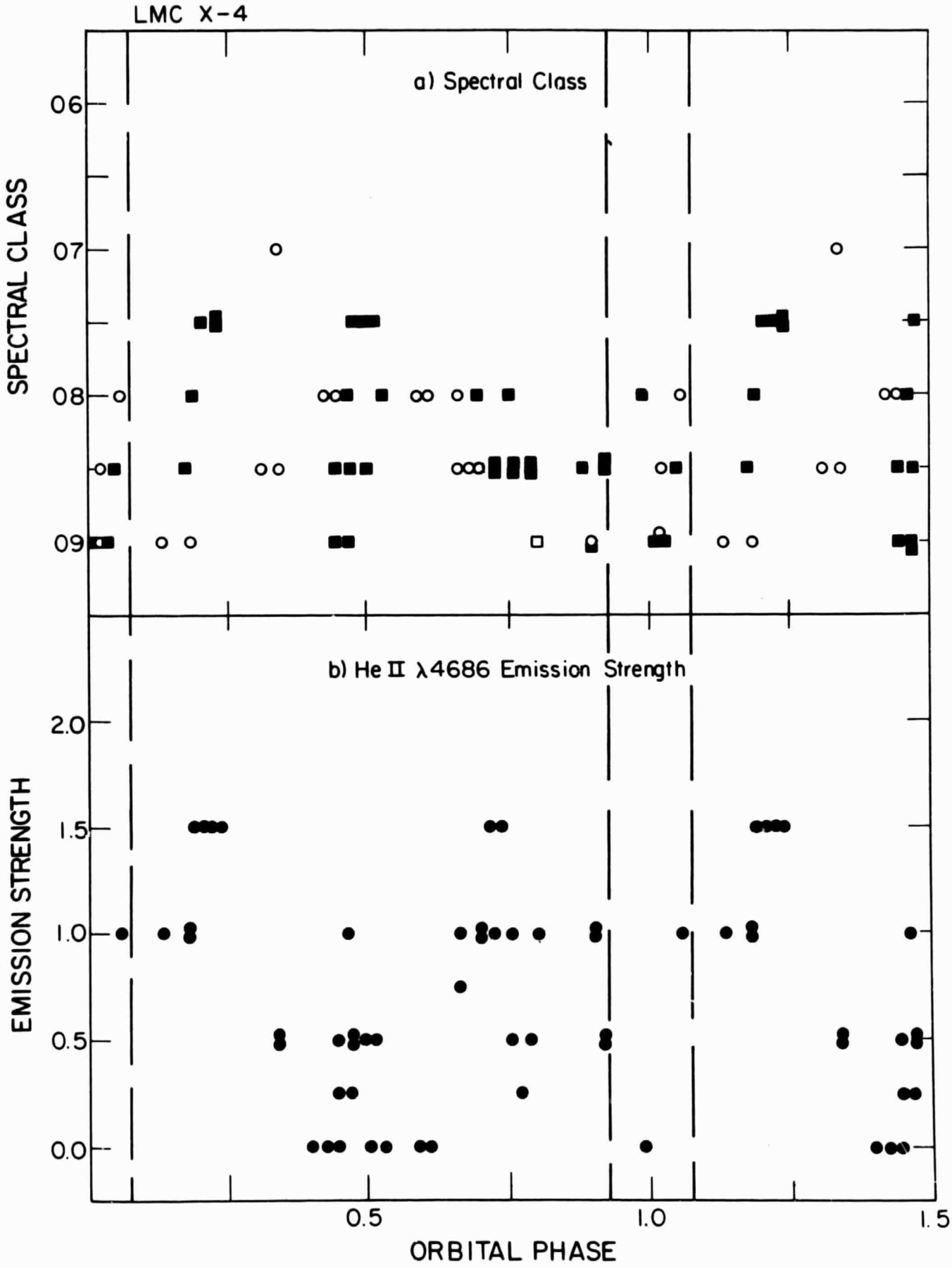
LMC X-4
a) Spectral Class
SPECTRAL CLASS
06
07
08
09
b) He II λ4686 Emission Strength
EMISSION STRENGTH
2.0
1.5
1.0
0.5
0.0
0.5
1.0
1.5
ORBITAL PHASE

Figure 3